Motion of microscopic grains in a periodic potential of plate acoustic waves

2003 J. Phys.: Condens. Matter 15 7201

(http://iopscience.iop.org/0953-8984/15/43/005)

INSTITUTE OF PHYSICS PUBLISHING JOURNAL OF PHYSICS: CONDENSED MATTER

J. Phys.: Condens. Matter **15** (2003) 7201–7211 PII: S0953-8984(03)63645-3

Motion of microscopic grains in a periodic potential of plate acoustic waves

A M Gorb, A B Nadtochii and O A Korotchenkov

Department of Physics, Kiev National University, Kiev 03680, Ukraine

Received 16 May 2003
Published 17 October 2003
Online at stacks.iop.org/JPhysCM/15/7201

Abstract

We report on a novel method of charge particle transport. It is based on the application of a moving electrostatic potential and an oscillating friction force to the particle which occur due to acoustic waves travelling in a piezoelectric medium. ZnS grains placed onto the surface of a Y-cut, Z-propagating $LiNbO_3$ plate experience a sequence of jumps in the forward and in the backward directions with respect to the phase velocity of the plate wave. The jump probability appears to change with the Lamb mode supported by the plate and the sign of the grain charge. We present computed spatial profiles of the piezoelectric potential and the displacement components on the surface of the plate for the two lowest resonant modes of Lamb waves. The occurrence of the grain motions is then explained by the presence of the electrical and friction forces, and good qualitative correspondence of the theory and experiment is found.

1. Introduction

Microscopic particles subjected to a periodic potential can experience a directional motion even if the average of an acting force remains zero [1]. Typically, an asymmetric external potential applied to Brownian particles is used to achieve Brownian ratchets. These have been extensively studied over the last decade due to their description of molecular motors. It has been illustrated that the ratchets can effectively transport micrometre- and millimetre-sized particles employing optical illumination [2] and electric fields [3, 4] to generate a driving force. Different types of acoustic waves have so far been employed to pump fluids adjacent to the wave transmitting medium [5]. The main features of the physics involved are due to acoustic streaming effect resulting from the production of a steady force by a harmonically varying mechanical displacement field acting at the boundary. With this technique, rotatory motors are known to exist [6, 7].

In this work, we have micromachined a piezoelectric-plate device allowing the transport of electrically charged micrometre-sized grains with a periodic potential of acoustic waves

0953-8984/03/437201+11$30.00

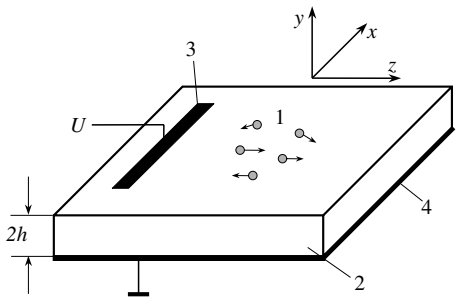

Figure 1. Schematic drawing of the transport device set-up. 1: ZnS grains, 2: $LiNbO_3$ plate, 3 and 4: metal electrodes.

which involves both the elastic displacement of the driving plate and the piezoelectric field influencing the motion of particles.

2. Experiment

Experiments were performed on two types of grains made of ZnS powders. The grains were electrically charged monopolarly using an electrophorus. In this study, we used two types of grains which carried opposite charges. Positively charged grains are referred to hereafter as grains of type 1 while negatively charged grains are referred to as grains of type 2. The charge was measured with an electroscope and its average value was found to be $+6 \times 10^{-15}$ and -5×10^{-16} Q per grain of type 1 and type 2, respectively. The particle diameters were measured by a light-scattering technique and were found to peak at about 13 and 5 μm for grains of type 1 and 2, respectively. The grains were essentially nonspherical and the shape anisotropy did not exceed $\approx$20%.

To form a transport device, the grains of a particular type (1 in figure 1) were placed onto the surface of a Y–Z $LiNbO_3$ piezoelectric plate (2 in figure 1). The device was illuminated with a bright light and placed on the translation stage of an optical microscope equipped with an image capturing technique. The results reported here correspond to a low-density regime and the grain motions (arrows in figure 1) matched closely a single-particle diffusion. It is believed that the observed motion was dominated by the interaction between the driving surface and the individual particles. This is contrasted with acoustically driven collective behaviour of grains in a dense particle system reported previously [8, 9].

Before proceeding with the experiments on the movement of grains we tested the propagation of acoustic waves in the plate. In order to excite the waves, we employed the method of two electrodes (3 and 4 in figure 1) previously discussed elsewhere [10]. The travelling z-propagating acoustic waves were excited in the driving plate by applying a radio-frequency (rf) voltage U to a 1 mm wide copper electrode (3 in figure 1) sputtered onto the face surface of the plate and a metallized bottom surface 4 connected to the ground. A similar electrode (not shown in figure 1) separated from the transmitter (3 in figure 1) by the length of the plate was used as a receiver of the transmitted wave. The resistance R_S of the exciting electrode, the electrostatic capacitance C_0 of the transducer and the tangent of the dielectric loss, $\tan\delta$, in $LiNbO_3$ were found to be 0.05 Ω, 12 pF and 10^{-3}, respectively. We used a matching inductance to match the radiation resistance of the transducer to the source resistance.

As discussed below, the y and z displacement components are coupled to the y component of the electric field, allowing piezoelectric coupling to Lamb wave modes. Two types of Lamb

wave modes can exist in isotropic, homogeneous plates: either symmetric or antisymmetric. At low frequencies, the lowest order symmetric (s_0) and antisymmetric (a_0) modes can propagate in the plate [11]. When the frequency increases above certain cut-off frequencies, the higher order resonant modes begin to propagate. The thickness of the plate used in the experiments was 630 μm, allowing the launch of low-frequency plate waves in the range from 2 to 6 MHz. The length of the plate in the direction of the travelling waves was 2 cm. In our experiments, we employed a 8-cycle toneburst as the input signal and wave modes with frequencies of 3.7 and 5.2 MHz. Signals from the receiving transducer were identified as being the first (at 3.7 MHz) and the second (at 5.2 MHz) resonant modes of Lamb waves by their group velocity as determined from the receiver separation and the burst transit times. In isotropic plates, these modes are usually defined as the first antisymmetric (a_0) and first symmetric (s_0) wave modes in terms of the particle displacements with respect to the mid-plate [11]. At the receiver, there also observed signals from another modes temporally separated from the dominant mode and a series of bursts originating from a multiply reflection at the plate boundaries. The ratio of averaged peak signal voltage for the dominantly excited mode to those of the other bursts was not smaller than 12 dB. Therefore, at the voltage U applied to move the grains, which was chosen to be only $\approx$10% larger than the threshold value for the observation of grain motions, the coexistence of many undesired bursts in the plate caused no difficulties in data interpretation.

Travelling waves produced grain hopping motions in all directions on the surface of the driving plate. We visually ascertained that the number of motions accomplished perpendicular to the z-direction was remarkably small, achieving its maximum values in the z- and in the $-z$-directions. A direct analysis of the images allowed us to estimate the relative probability of the angle-averaged forward and backward displacements of the grains. We count the number of forward (N_f) and backward (N_b) grain motions as a function of the hop length along the z-axis. The forward probability is then $P_\mathrm{f} = N_\mathrm{f}/N$ and the backward one is $P_\mathrm{b} = N_\mathrm{b}/N$ with the total number of jumps $N \geqslant 200$.

All experiments presented here were performed at ambient temperature and pressure.

3. The driving potential

This section serves as a motivation of the driving potential used to explain our experimental results. We first discuss the displacements and electric fields accompanying the plate waves and then provide a general framework of acoustic pumping effect for the detailed treatment of the experimental results in section 4.

3.1. Displacement components and electrostatic potential at the surface of a $LiNbO_3$ plate

In a piezoelectric elastic medium, acoustic waves are described by the three-component displacement field u_i and the electrostatic potential φ [12]:

$$\rho \frac{\partial^2 u_i}{\partial t^2} = \frac{\partial T_{ij}}{\partial x_j}, \tag{1}$$

$$\frac{\partial D_i}{\partial x_i} = 0, \tag{2}$$

$$T_{ij} = c_{ijkl} \frac{\partial u_k}{\partial x_l} + e_{mij} \frac{\partial \varphi}{\partial x_m}, \tag{3}$$

$$D_i = e_{ikl} \frac{\partial u_k}{\partial x_l} - \varepsilon_{ij} \frac{\partial \varphi}{\partial x_j}, \tag{4}$$

where **T** is the stress tensor, **D** is the electric displacement vector, c_{ijkl} are the elastic moduli of the medium, e_{mij} are its piezoelectric coupling coefficients, ε_{ij} is the tensor of the dielectric constants, ρ is the mass density and repeated indices are summed.

We now consider a Y-cut, Z-propagating (Y–Z) $LiNbO_3$ plate of thickness $2h$ and with the z-axis as the wave propagation direction; see figure 1. The back face of the plate is metallized. Equations (1)–(4) must be solved subject to the mechanical and electrical boundary conditions at the plate surfaces and $\nabla^2\varphi = 0$ everywhere outside the plate. The mechanical boundary conditions are

$$T_{2i}(\pm h) = Z_i \omega u_{si}, \tag{5a}$$

where Z_i is the impedance of the adjoining medium (air) for the ith component of the surface displacement u_{si} and ω is the angular frequency. In writing equation (5a), we neglected the mechanical coupling between the $LiNbO_3$ plate and the metal layers. Furthermore, since the adjoining medium's impedance is much smaller than that of the $LiNbO_3$ plate we approximate the mechanical boundary conditions by

$$T_{23}(\pm h) = T_{22}(\pm h) = T_{21}(\pm h) = 0. \tag{5b}$$

The electrical boundary conditions can be written as

$$D_2(+h) = -\varepsilon_a \varepsilon_0 \frac{\partial \varphi}{\partial y}, \qquad \varphi(-h) = 0, \tag{6}$$

where $\varepsilon_a \approx 1$ is the dielectric constant of the adjoining medium.

The plane-wave solutions of equations (1)–(4) are assumed to be of the form

$$u_i = u_{0i} \exp[\mathrm{i}k(Vt - z - \beta y)], \tag{7a}$$

$$\varphi = \varphi_0 \exp[\mathrm{i}k(Vt - z - \beta y)]. \tag{7b}$$

In this notation u_{0i} and φ_0 are the amplitude of the displacement components and the electrostatic potential, respectively, k is the wavevector, V is the phase velocity of the wave and β is the decay constant. Substitution of equations (7) into (1)–(4) gives the determinantal eight-order equation in β with velocity V as an unknown parameter [13]. For every value of V, there are eight solutions β_n, so that the displacement field and the electrostatic potential are given by

$$u_i = \sum_{n=1}^{8} u_{0in} \exp[\mathrm{i}k(Vt - z - \beta_n y)], \tag{8a}$$

$$\varphi = \sum_{n=1}^{8} \varphi_{0n} \exp[\mathrm{i}k(Vt - z - \beta_n y)], \tag{8b}$$

where $u_{0in} = \varphi_{0n} u_{in}$. One then has to satisfy the boundary conditions (5) and (6) yielding a set of eight homogeneous algebraic equations. To obtain a nontrivial solution it is required that the determinant of an 8×8 matrix $M(m, n)$ given by

$$\begin{aligned}
M(1,n) &= \exp(kh\beta_n)[u_{xn}(c_{66}\beta_n + c_{14})] \\
M(2,n) &= \exp(-kh\beta_n)[u_{xn}(c_{66}\beta_n + c_{14})] \\
M(3,n) &= \exp(kh\beta_n)[u_{yn}(c_{11}\beta_n - c_{14}) + u_{zn}(-c_{14}\beta_n + c_{13}) + e_{22}\beta_n + e_{31}] \\
M(4,n) &= \exp(-kh\beta_n)[u_{yn}(c_{11}\beta_n - c_{14}) + u_{zn}(-c_{14}\beta_n + c_{13}) + e_{22}\beta_n + e_{31}] \\
M(5,n) &= \exp(kh\beta_n)[u_{yn}(-c_{14}\beta_n + c_{44}) + u_{zn}c_{44}\beta_n + e_{15}\beta_n] \\
M(6,n) &= \exp(-kh\beta_n)[u_{yn}(-c_{14}\beta_n + c_{44}) + u_{zn}c_{44}\beta_n + e_{15}\beta_n] \\
M(7,n) &= \exp(kh\beta_n)[u_{yn}(e_{22}\beta_n + e_{15}) + u_{zn}e_{15}\beta_n - (\varepsilon_{11}\beta_n + \mathrm{i}\varepsilon_0)] \\
M(8,n) &= \exp(-kh\beta_n)
\end{aligned} \tag{9}$$

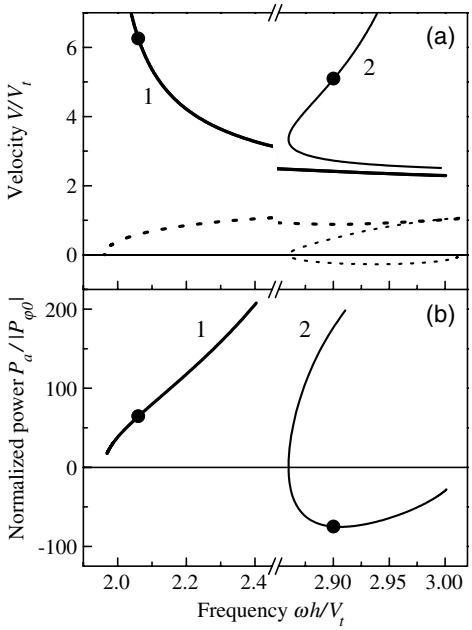

Figure 2. Computed dispersion curves for a Y–Z $LiNbO_3$ plate (a) and dependence of acoustic power flow on normalised frequency $\omega h/V_t$ (b) for the first (1) and second (2) resonant mode of Lamb waves. Dotted curves show the group velocity as a function of $\omega h/V_t$. $V_t = \sqrt{c_{44}/\rho} = 3573$ m s^{-1}. Points indicate the parameters employed in the experiments.

be equal to zero. The search procedure was used to satisfy the above conditions resulting in the dispersion curves for V shown in figure 2(a). Obviously, matrix (9) implies the existence of two types of plate waves in Y–Z lithium niobate. The displacements in the Lamb waves are confined to the yz plane, and the plate waves with the u_x component are referred to as the horizontal shear mode waves. In this study, we employed the Lamb modes of plate waves, so that the u_x component is presumed to be zero. It may also be deduced from matrix (9) that the yz displacement component is coupled piezoelectrically to the y component of electric field, as pointed out in section 2. The computed particle displacement fields are shown in figure 3 for the two lowest resonant Lamb wave modes employed in the experiments. It is seen that the dilatation and contraction patterns are seemingly antisymmetric with respect to the mid-plate in the first resonant mode ((a) in figure 3). In contrast, they resemble the symmetrical case in the second resonant mode displayed in figure 3(b). By using the material parameters for $LiNbO_3$ [12] we obtain the piezoelectric potential φ at the surface of the plate and the surface displacement components u_y and u_z for the two lowest Lamb wave modes exhibited in figure 4.

Using equation (8) it is possible to relate the values of the displacement components u_i to that of the potential φ. In order to estimate the amplitude of the electrostatic potential φ_s at the surface of the plate, we need to relate the acoustic power P_a carried by the plate wave in the z-direction to the electrical rf power P_e given by

$$P_e = \tfrac{1}{2} U I \cos(\Delta\phi), \tag{10}$$

where U is the applied rf voltage, I is the rf current feeding the plate and $\Delta\phi$ is the phase difference between the two. In order to arrive at a simple expression we impose a physical constraint by requiring that the average acoustic power flow in the direction of propagation be unchanged over the plate length. Therefore, based on available studies of surface acoustic

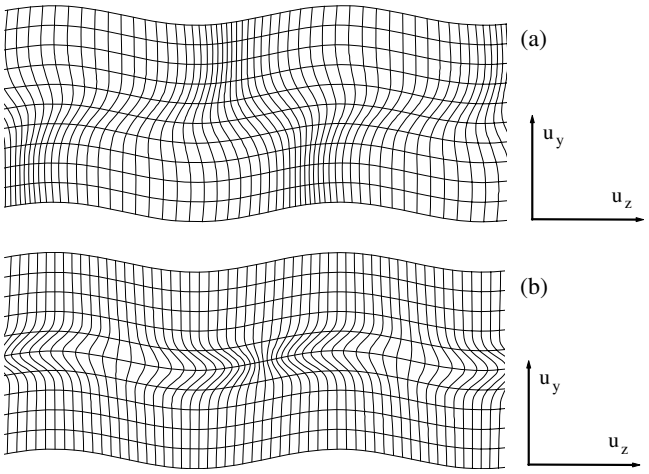

Figure 3. Displacement field distributions for the first (a) and second (b) resonant Lamb wave modes.

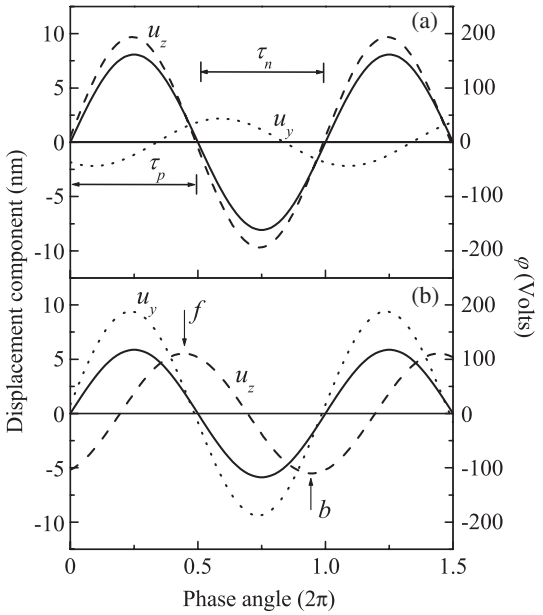

Figure 4. Computed piezoelectric potential (solid curves) and displacement components (dotted curves) on the surface of a Y–Z $LiNbO_3$ plate induced by the first (a) and second (b) resonant mode of Lamb waves plotted as a function of the phase angle $k(Vt - z)$.

waves in $LiNbO_3$ [14], we are tempted to argue that the mechanical loss in the low-frequency range employed in this study may safely be assumed to be zero. We furthermore suggest that the dielectric loss as well as the loss determined by metal electrode resistivity are presumed to be nearly zero. The latter assumption is based on the fact that the radiation resistance ($\approx 10^2\ \Omega$) of the transmitter is much larger than $R_S + (1/\omega C_0) \tan\delta \approx 3\ \Omega$. These constraints obviously amount to a slightly overestimated value of φ. However, they seem plausible for comparing

the experimental data presented in section 4 with the model developed in section 3. Hence we write

$$P_a = 0.5P_e, \tag{11}$$

implying that the wave is launched both in the z- and $-z$-directions.

The time average acoustic power flow in the j-direction can be written as [15]

$$P_j = \tfrac{1}{2}\,\mathrm{Re}(\dot{D}_j\varphi^* - T_{ij}\dot{u}_i^*), \tag{12}$$

where the asterisks indicate the complex conjugate and the dot denotes differentiation with respect to time. Noting that $\varphi = 0$ at $y \leqslant -h$, the acoustic power P_a becomes the sum of three terms,

$$P_a = P_u + P_\varphi + P_{\varphi 0} = \tfrac{1}{2}w\,\mathrm{Re}\left(\mathrm{i}\omega\int_{-h}^{+h}(T_{32}u_y^* + T_{33}u_z^*)\,\mathrm{d}y\right) + \tfrac{1}{2}w\,\mathrm{Re}\left(\mathrm{i}\omega\int_{-h}^{+h}\varphi^* D_z\,\mathrm{d}y\right)$$
$$+ \tfrac{1}{2}w\,\mathrm{Re}\left(\mathrm{i}\omega\int_{+h}^{+\infty}\varphi^* D_z\,\mathrm{d}y\right), \tag{13}$$

representing the time average mechanical (P_u) and electrical (P_φ and $P_{\varphi 0}$) components of the total power P_a transmitted within the plate (P_u and P_φ) and in the free space ($P_{\varphi 0}$). Here w denotes the wave aperture and $\omega = kV$. Using the dispersion curves and performing the numerical integration we obtain the frequency dependence of P_a displayed in figure 2(b) for the two lowest Lamb modes which are used in the experiments.

These modes are shown by circles in figure 2(a) indicating that the electrostatic potential φ travels in the direction of the acoustic power flow (i.e. the phase and the group velocities of the wave are in the same direction) at the lower-frequency mode (curve 1) whereas, at the higher-frequency mode, it in turn travels backwards (the phase and the group velocities of the wave are in opposite directions in curve 2). In equation (13) the power may be written in the much simpler form

$$P_a = M\varphi_s^2, \tag{14}$$

and

$$P_{\varphi 0} = -\tfrac{1}{4}w\varepsilon_0\omega\varphi_s^2, \tag{15}$$

where ε_0 is the vacuum permittivity and M is a coefficient. Combining equations (14) and (15) M becomes

$$M = \tfrac{1}{4}w\varepsilon_0\omega\frac{P_a}{|P_{\varphi 0}|}. \tag{16}$$

Therefore, using the data of figure 2(b) the value of M may be obtained for a specific wave frequency. From equations (10), (11) and (14) we then obtain

$$\varphi_s = \sqrt{\frac{UI\cos(\Delta\phi)}{4|M|}} \tag{17}$$

yielding a value of the peak potential displayed in figure 4.

3.2. Principles of acoustic pumping

Consider the data of figure 4(a). As the u_y displacement component is remarkably smaller than the u_z component the motion of a charged particle placed on the surface of a $LiNbO_3$ plate at a given z may be considered to be essentially one-dimensional. The particle is influenced by two periodic forces. One of them is due to friction between the grain and the driving surface

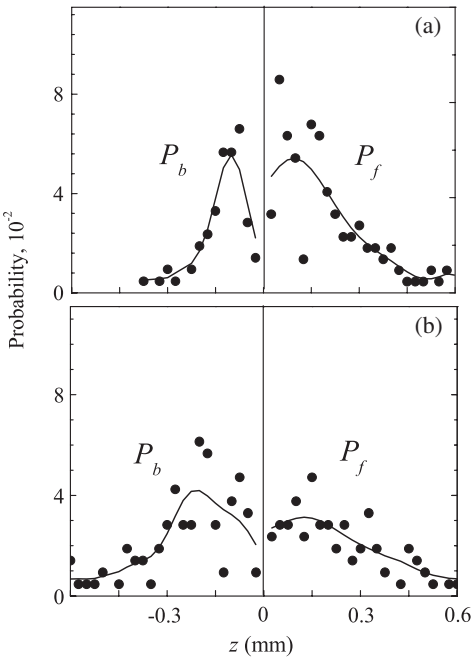

Figure 5. Probabilities P_f and P_b for a positively charged particle to hop forwards and backwards, respectively, as a function of the hopping length. The frequency is (a) 3.7 and (b) 5.2 MHz. The points are experimental data; the curves act as a guide to the eye.

mimicking the fluctuating friction force acting to the particle. The other one is of electrical origin.

In the simplest theoretical picture, a positively charged particle is bounded at the plate surface by the electric trapping force during the negative cycle (τ_n) of the electrostatic potential. Therefore, the probability P_b of the particle motion in the backward direction (negative values of u_z in figure 4(a)) may be considered to be much smaller than the forward motion probability P_f. The forward motion is maintained during the positive cycle of u_z (cf τ_p in figure 4(a)) when a positively charged particle is unbound by the positive cycle of φ. In contrast, a negatively charged particle would be expected to give $P_\mathrm{b} > P_\mathrm{f}$. One should, however, keep in mind that there always exists a drift force pulling the particles in the direction of the travelling potential thus influencing the total number of the particle motions in a given direction.

It is evident in figure 4(b) that at the higher-mode Lamb wave, the forward and the backward motion probabilities (arrows f and b) attain their maximum values when the potential φ tends to zero. Therefore, $P_\mathrm{b} \approx P_\mathrm{f}$.

One thus concludes that there exists a phase difference between the piezoelectric potential and the displacement field which can easily be varied by tuning the frequency of the plate wave. This may significantly affect the forward and the backward motion probabilities for microscopic particles placed on the surface of the plate. The effect is furthermore sensitive to the particle charge.

4. Experimental results and discussion

The most significant results are displayed in figures 5 and 6. Note that applied voltage $U = 55$ V for panels (a) and $U = 50$ V for panels (b) in figures 5 and 6 are commensurate with the potential

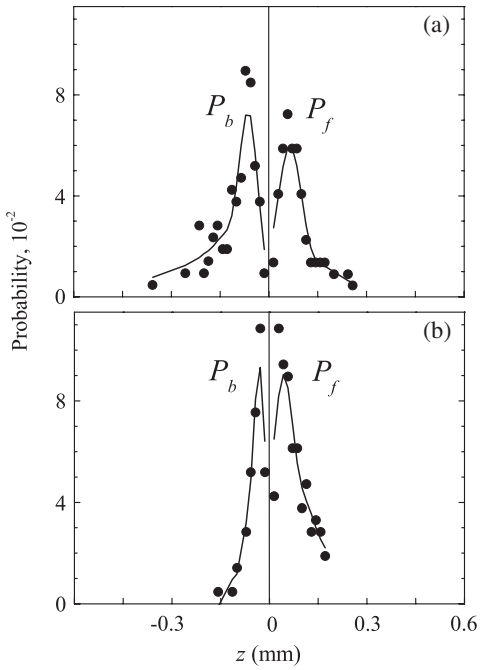

Figure 6. The same as in figure 5 but for a negatively charged particle.

and displacement amplitudes shown in figure 4. As is seen in figure 5(a), positively charged particles (type 1 grains) driven at the first resonant mode of Lamb waves appear to be better transported in the forward direction than in the backward direction. As noted above, the sign of the particle charge has a profound impact on the probability distribution. We find markedly enhanced $P_{\rm b}$ probability at the expense of the $P_{\rm f}$ for negatively charged grains (type 2); see figure 6(a). Thus, the quantity $P_{\rm f}$ obtained from the square of the plot displayed in figure 6(a) is found to be roughly 0.4 of that in figure 5(a) while that for $P_{\rm b}$ is about 1.2. These findings are remarkable in that they are appealingly consistent with the simple theory pointed out in section 3.2.

To get further insight within the suggested model, one should take into account the drag force acting on the grain in the direction of the travelling potential. This may be done by employing an effective potential,

$$\varphi_{\rm eff}(z) = \varphi(z) - zF, \tag{18}$$

experienced by the particle. Physically, it accounts for the occurrence of the acoustoelectric force F [16] which is proportional to the rf power delivered to the $LiNbO_3$ plate. We thus have a tilted washboard potential with a periodic array of traps for a charged particle travelling at a constant velocity V along the z-axis. Significantly, a positive force $F > 0$ arises at the lowest resonant Lamb mode and pulls the particles in the forward direction. Hence, the effective potential is tilted to the right in figure 7(a). A negative force $F < 0$ arising at the second resonant mode of Lamb waves and pulling the particles backwards corresponds to a washboard tilted to the left as shown in figure 7(b). In our experiments, the force trapping the grains in the potential minima (for positively charged grains) or maxima (for negatively charged grains) appears to be too small to drag them in the forward or backward direction. Therefore, grain motions can be understood as being due to the forward (or backward) drag

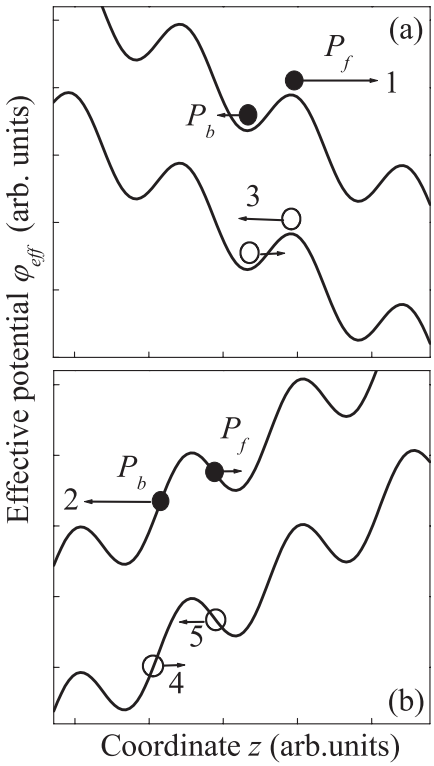

Figure 7. Effective potential $\varphi_{\rm eff}$ for the first (a) and second (b) Lamb wave mode (see the text for details). Closed and open circles display positively and negatively charged grains, respectively. Arrows schematically illustrate the motion probability in the forward (rightward arrows) and backward (leftward arrows) directions.

force and the fluctuating mechanical force acting on the particle. The former pulls the particles forwards (or backwards) while the latter leads to the grain hops, even in the direction opposite to that of the velocity V.

Consistent with the notions argued in section 3, the hopping probabilities $P_{\rm f}$ and $P_{\rm b}$ may be schematically approximated by the length of the arrows sketched in figure 7. For a positively charged grain of type 1 (closed circles in figure 7) the probability $P_{\rm f}$ to hop forwards is remarkably large at the first resonant mode (arrow 1 in figure 7) while at the second Lamb mode the backward jump probability turns out to enhance (arrow 2 in figure 7). As a consequence, the number of motions with $z > 0$ seen in figure 5(a) drops in figure 5(b) at the expense of the backward motions with $z < 0$. Furthermore, the backward probability $P_{\rm b}$ broadens remarkably in figure 5(b) compared with the one displayed in figure 5(a), which likewise is reminiscent of the broad $P_{\rm f}$ distribution shown in figure 5(a). Evidently, an enhanced number of long jumps in the forward direction in figure 5(a) and in the backward direction in figure 5(b) is corroborated theoretically by an increased motion probability due to the tilted effective potential; see the upper curves in figures 7(a) and (b).

In contrast, for a negatively charged grain of type 2 (open circles in figure 7) the phase difference between the electrical and mechanical forces does not imply enhanced hopping probabilities (arrows in the lower curves of figures 7(a) and (b)). As a consequence, the jump distributions remain remarkably narrow in figure 6. More precisely, short jumps are most

probable in the backward direction in figure 7(a) (arrow 3) giving rise to a larger P_b probability in figure 6(a) in comparison with the other motion probabilities displayed in figure 6. As the φ_{eff} potential is reduced leftwards in figure 7(b) barriers appear to exist for both the forward and the backward motions (arrows 4 and 5) taken at the second resonant mode. A narrowed P_b distribution is then observed in figure 6(b) compared with that shown in figure 6(a). As expected, the value $P_b/P_f \approx 1.4$ in figure 6(a). On the other hand, P_b in figure 6(b) is only about 0.5 of the one in figure 6(a).

We thus conclude that the suggested model employing two forces acting on the particle works well. Therefore, this theory and experimental results qualitatively demonstrate a new perspective on extending acoustic driving techniques.

5. Conclusions

Travelling acoustic waves produce a pumping of grains across the surface of the driving plate. The grain motions are observed to be single hopping events, and the probability distribution for the forward and for the backward particle jumps depends on the frequency of the plate wave and the grain charge. This behaviour is in good agreement with a simplified model describing the occurrence of the grain motion in the presence of the moving piezoelectric field and surface displacements interacting with the grain via a tilted electrostatic potential and via friction, respectively.

We believe that the employment of a periodic potential of acoustic plate waves can be profitable in different fields, which are beyond the scope of the present study. In particular, developing new acoustic driving techniques should be of great significance in providing a pump or separation component for charged molecular species in biology, allowing the implementation of an acoustically driven device microfabricated on a single chip. The size of the device and the size of the transported fragments may be adjusted by tuning the employed frequency range.

References

[1] For a recent review, see Reimann P J 2002 *Phys. Rep.* **361** 57
[2] Faucheux L P, Bourdieu L S, Kaplan P D and Libchaber A J 1995 *Phys. Rev. Lett.* **74** 1504
[3] Rousselet J, Salome L, Ajdari A and Prost J 1994 *Nature* **370** 446
[4] Gorre L, Ioannidis E and Silberzan P 1996 *Europhys. Lett.* **33** 267
[5] Moroney R M, White R M and Howe R T 1991 *Appl. Phys. Lett.* **59** 774
[6] Ueha S 1989 *Proc. IEEE Ultrasonics Symp.* (New York: IEEE) p 749
[7] Kenjo T and Sashida T 1993 *Introduction to Ultrasonic Motors* (Oxford: Clarendon)
[8] Korotchenkov O A and Goto T 1997 *Phys. Rev.* B **56** 13646
[9] Gorb A N and Korotchenkov O A 2002 *Technol. Phys. Lett.* **28** 740
[10] Kucherov I Ya and Ostrovskii I V 1969 *Fiz. Tverd. Tela* **11** 2373
[11] Victorov I A 1967 *Rayleigh and Lamb Waves: Physical Theory and Applications* (New York: Plenum)
[12] Dieulesaint E and Royer D 1980 *Elastic Waves in Solids* (Chichester: Wiley)
[13] Joshi S G and Jin Y 1991 *J. Appl. Phys.* **70** 4113
[14] Matthews H (ed) 1977 *Surface Wave Filters* (New York: John and Sons)
[15] Milsom R F, Reilly N H C and Redwood M 1977 *IEEE Trans. Sonics Ultrason.* **24** 147
[16] Mason W P (ed) 1966 *Physical Acoustics* vol 4A (New York: Academic)